On the life and habits of gas-core slugs: characterisation of an intermittent horizontal two-phase flow

Yessica Arellano, Andrew Hunt, Olivier Haas and Yu Ma

Original citation & hyperlink:
Arellano, Yessica, et al. "On the life and habits of gas-core slugs: characterisation of an intermittent horizontal two-phase flow." *Journal of Natural Gas Science and Engineering* 82 (2020): 103475.
https://dx.doi.org/10.1016/j.jngse.2020.103475

DOI 10.1016/j.jngse.2020.103475
ISSN 1875-5100

Publisher: Elsevier

On the life and habits of gas-core slugs: characterisation of an intermittent horizontal two-phase flow

Yessica Arellano, Andrew Hunt, Olivier Haas, Lu Ma

***Abstract* —Slugs are intermittent structures observed in horizontal co-current gas-liquid two-phase flow. Published data examining horizontal flow indicate the existence of intermittent sub-flow patterns. There is limited work performed on the study of this sub-categorisation. This paper presents a method, exploiting non-intrusive Electrical Capacitance Tomography (ECT) measurements, to assess and to characterise the spatial and temporal features of horizontal gas-oil flow. A logic-based algorithm is proposed to automatically identify and classify flow regimes. This algorithm uses the spatial distribution of the phases, based on measurements of the intrinsic dielectric properties of the fluids. The measurements were performed at the NEL UK national standard multiphase flow loop using a high-speed dual-plane ECT sensor array. The ECT measurements identified intermittent liquid structures with a sustained gas-core in the central region of the pipe cross-section with outer features analogous to those of liquid slugs. Assessment of the frequency and time span of the periodic structures showed that gas-core slugs are, typically, shorter than full slug structures but are more frequent for the same given time period. For both flow structures, the mixture velocity was a determinant factor, with gas-core slugs dominating the flow at higher velocities. The experimental work led to the modification of existing flow pattern transition models. The modified flow regime maps suggested in this study aim to widen the applicability of the results by enabling the prediction of gas-core slug flow for similar experimental and operating conditions. The present work comprises the initial steps towards automatic flow regime identification in multiphase flow metering. Automatic flow regime recognition has the potential to lead to better process control and improved accuracy in production allocation.**

***Keywords*— Slug, Gas-core slug, pattern recognition, electrical capacitance tomography, multiphase flow**

Paper submitted for review on the 06/03/2020.

Y. Arellano is with the Fluid and Complex Systems Center, Coventry University, CV1 2NL, England (e-mail: prietoy@ uni.coventry.ac.uk).
A. Hunt is with iPhase Ltd, Basingstoke, RG24 8NE. England. (e-mail: andyhunt@iphaseflow.com).
O. Haas is with the Institute for Future Transport and Cities, Coventry University, CV1 5FB. England. (e-mail: Olivier.haas@coventry.ac.uk).
L. Ma is with iPhase Ltd, Basingstoke, RG24 8NE. England. (e-mail: luma@iphaseflow.com).

1. Introduction

Multiphase flow measurement aims to quantify the flowrates of the fluids flowing through a pipe. The spatial distribution of the fluids in the pipe can significantly impact the accuracy of the meters [1]. The latest multiphase flow measurement technologies use flow pattern identification techniques combined with artificial neural network to increase the measurement accuracy of the flow meters [2]. Prediction of flow patterns of gas-liquid flows in pipelines are usually based on the flow pattern maps that are available in the literature. Flow pattern maps are typically derived from experimental observations via optical methods under controlled conditions. The visual characterisation of flow configurations offers an insight into the distribution of fluid species inside a pipeline for given operational conditions.

Commonly, flow classification depends on two main conditions, namely; the fluid species and the flow direction. Regarding the former, the multiphase flows can be characterised based on the phase distribution of the gas-liquid or of the liquid-liquid species within the pipeline for a given range of operating conditions. The spatial distributions of the gas-liquid phases within a horizontal pipe can be described as an evolution of patterns. At low flow velocities, the fluids tend to segregate and flow in separate strata, denoted stratified flow. In stratified flow, gravity effects yield the denser phase to flow at the bottom section of the pipe while the gas occupies the top section. As the gas velocity increases, the inertial forces dominate over viscous forces, and waves are formed in the interphase, yielding stratified wavy flow [3]. With increasing gas velocity, the size of the waves increases, reducing the available area for gas flow. This area reduction increases even further the gas velocity and causes an instant drop in pressure. This phenomenon yields large irregular waves that can reach the top of the pipe resulting in intermittent patterns of alternating stratified flow and slugs of liquid. Alternatively segregated stratified flow can transition to segregated annular flow, or to distributed flow, depending on the conditions of the liquid as reported by [4] [5] [6] [7]. This three-way transition region between stratified, intermittent and annular flow that yields a pseudo-slug area, as identified by Lin and Hanratty [8], has not been sufficiently addressed in the literature. Even though horizontal pseudo-slugs has gained increasing attention in recent years, there is no general agreement on the characteristics of a pseudo-slug [9][10][11][12][13]. A study in air-water horizontal flow found that two spatial structures coexist in that pseudo-slug zone [14]. In one type of structure, the air penetrates through the water forming a two-phase mixture in the core of the slug with no clear boundary between the phases, and in the other, the air forces the water to the pipe perimeter with a gas-continuous core. For consistency, in the remainder of this manuscript, the pseudo-slug with a maintained gas core is referred to as '*gas-core slug*', as denoted by [15]. Note that gas-core slugs are consistent with structures previously reported as 'ghost' or 'huge waves' [14] [16]. This phenomena will be addressed in detail in this manuscript with the aim of gaining more knowledge on this recently studied sub-flow pattern. This is achieved by extending the analysis to fluids of interest for hydrocarbon transportation.

Characterisation of multiphase flow in pipelines has undergone significant research in previous years resulting in numerous flow pattern maps. The generalisations used for the development of pattern maps are based on the use of correction factors for given fluid properties [6], the ratio of superficial velocities [17] [18] [19], or through dimensionless numbers [5] [20] [21]. The identification of dynamic flow regimes is an empirical process usually done via visual observation of the flow spatial arrangements. The flow regimes are discretised based on intermittency, scale and structure. This process is time-consuming and observations are limited to what can be seen through a transparent pipe wall. The drawback of optical techniques is that complex or detailed flow configurations that are not visible using the human eye or machine vision could be misinterpreted. Examples of flow structures whose externally visible assembly may not be entirely representative of the overall flow configuration include fluids with significant bubble structures or opaque fluids and, in particular, oilfield multi-phase flows [22].

Several data processing techniques have been developed to improve flow characterisation, including a) statistical analysis of traditional sensor data, b) statistical analysis of image data, and c) combined statistical and structure analysis of image data. These techniques, while valuable in studying the flows are often either frequency-limited with non-specific sensitivity [23] or they are non-physical where the link to conventional patterns is not clear. For combined analysis, it is possible to identify key physical parameters and apply statistical techniques. While this method shows great promise, standard procedures have not currently been agreed [24]. Alternatively, flow pattern characterisation can be investigated using different hardware systems. Some of the most widely used methods comprise techniques and elements that are either intrusive e.g. quick-closing valves [25] and wire-mesh sensors [14], or contain nuclear sources e.g. gamma-ray densitometers [16]. Intrusive techniques have the drawback that they interact with the process and can perturb the flow yielding to misleading observations. In this work the capabilities for flow pattern identification via contactless tomography techniques are exploited. This approach enables flow regimes to be evaluated directly and accurately from on-line tomographic measurement systems which are therefore not extrapolations from laboratory data but from real-time measurements.

Although the method developed in the present manuscript can be applied to measurements from any tomography system, Electrical Capacitance Tomography (ECT) is used due to its suitability regarding the nature of the multiphase mixture, i.e. non-conductive fluids with distinct dielectric properties. ECT is a non-intrusive imaging technology based on the measurement of the dielectric properties of the fluids inside the pipe. The permittivity distribution within the pipe allows the direct computation of the volumetric concentration of the gas and oil phases along the pipe cross-section [26]. The capabilities of ECT for two phase measurements have been assessed by comparing ECT to gamma-ray densitometers [16], and wire-mesh sensor [27]. Consequently, ECT has been used to obtain images of the distribution of permittivity inside pipelines transporting non-conductive flows [28] [29] [30] [31] [32] [33] [34]. These studies have shown that measurement of dynamic properties of local flow, in addition to being non-intrusive, are fast and accurate, although with low spatial resolution.

The analysis of the experimental data presented in this study aims to provide a better understanding of the transition boundaries between the flow regimes and their relationship with dimensionless parameters. The combination of tomography imaging and an automatic pattern recognition algorithm is used here for the first time, resulting in a characterisation of gas-core slugs with relevant implications in flow pattern prediction and measurement accuracy. Improved accuracy of flow regime prediction yields potential cost reduction associated with transport and production handling costs. The automatic flow regime identification proposed here can be applied directly to improve process measurement, modelling and real-time control. Additionally, the derivations of improvements to non-dimensional maps for a broader flow characterisation can be of significant impact for oil field operators, and facilities designers.

The remainder of this paper is organized into four sections as follows. Section 2.1 provides an overview of horizontal gas-liquid flow patterns and proposes a unified horizontal gas-liquid flow pattern characterisation based on published literature. Section 3 details the methodology under which the tests were conducted and the data was analysed. The automatic flow pattern algorithm based on combined mean concentration from reconstructed images is also detailed in Section 3. Section 4 exploits the capabilities of ECT for the flow regime identification based on temporal and spatial key parameters. The characterisation of the intermittent flow structures, provided in Section 4, serves to predict regime transitions and propose changes to existing flow pattern maps. Finally, in Section 5, the main remarks of this study are drawn.

2. Theory

2.1 Horizontal Flow Regime Characterisation

In the literature, diverse flow regime classifications for gas-liquid mixtures can be found. As a result, a large number of different definitions arise, which complicates the comparison of performance of the existing flow regime maps. Three main flow patterns are regularly found in horizontal gas-liquid flow mapping, namely: (1) segregated flow where both phases are separated into two (stratified) or three layers (annular), (2) dispersed flow where droplets of liquids or gas bubbles travel through the matrix of the continuous phase, and (3) intermittent flow. An integrated flow pattern classification would enable cross-correlation among different studies. The unified classification proposed in Table 1, based on the existing classifications, constitutes the initial basis for the present study.

The vast majority of flow maps in the literature were constructed based on correlating the dimensional quantities of the experimental data and visual observations of the flow regimes developed. The use of dimensional quantities, although advantageous and broadly used, limits the applicability of the maps to conditions similar to those at which they were derived, e.g., flow properties and pipe dimensions [35]. Conversely, the use of dimensionless numbers to predict flow pattern distribution

Table 1. Unified horizontal gas-liquid flow pattern classification

Flow Pattern	Characteristics	Representation
Distributed – Bubble	-The liquid forms a continuous phase with dispersed bubbles of gas.	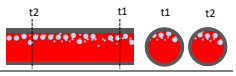
Distributed – Mist	- Most or all of the liquid is entrained by the gas phase.	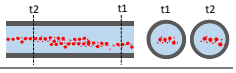
Intermittent – Slug	-Periodic waves reach the top of the pipe. -The flow consists of slugs of liquids alternated with segregated flows.	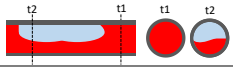
Intermittent – Plug	-Alternate plugs of liquid and gas move along the upper section of the pipe.	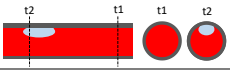
Intermittent – Gas-core slug	- Periodic waves reach the top of the pipe. -The flow consists of gas-core slugs of liquids alternated with segregated flows.	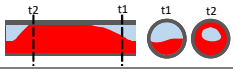
Segregated – Stratified	- Flow in separate layers. The liquid flows at the bottom of the pipe. - The gas flows at the top of the pipe. - The interface is flat	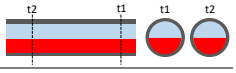
Segregated – Wavy	- Flow in separate layers. The liquid flows at the bottom of the pipe. - The gas flows at the top of the pipe. - Visible waves in the interface.	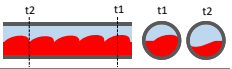
Segregated – Annular	- The gas flows through the pipe core. -The liquid forms film layer around the pipe walls. Due to gravity the film at the top of the pipe is thinner than at the bottom.	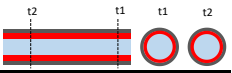

provides the opportunity of extended applicability to a wider range of conditions since they correlate the forces governing the phenomena and the effect of variations in the fluid properties.

In this work, the prediction accuracy of eight flow pattern maps for data collected through gas-liquid flow experiments is evaluated. The map selection was made considering (a) proven extrapolation to different data sets, (b) spread of industrial use, and (c) applicability to the experimental conditions for our data. In this sense, the assortment of selected maps accounts for the above consideration and all three generalisations detailed before, i.e., correction factors, ratio of superficial velocities and dimensionless numbers.

The regime classifications assessed here comprise those derived by Beggs and Brill [4], Beggs and Brill modified [35], Shell [20], Eaton [5], Baker [6], Taitel-Dukler [3], Barnea [7], Lin and Hanratty [8], and NEL [36] [37] (See Appendix). The latter corresponds to the flow regime map from the experimental facility where experiments were undertaken. The maps from Beggs and Brill, Beggs and Brill modified, and Eaton account for a combination of dimensionless quantities and the Froude number. The Froude number derives ratio of inertial force to the gravity force acting on the fluid, which is highly relevant for wave structures and hence the regime transition between segregated and intermittent phases. The maps from Shell, Lin and Hanratty, and Beggs and Brill, do not consider the effect of varying the fluid properties in the flow regime transitions. In opposition to this, the maps from Baker and that of Eaton consider the density, viscosity and surface tension of the phases. To supplement the study, the semi-theoretical approach from Taitel-Dukler, which does not follow any of the generalisations above, was also included.

2.2. Sketch of gas-core slug structures

Prior to flow pattern characterisation, it is necessary to introduce the intermittent flow distribution of gas-core slugs (GCS). The sequence of the volume fraction distribution in the cross-section of the pipe when intermittent structures flow through the ECT measurement plane, together with the cumulative volumetric fraction is shown in Fig. 1. The oil fraction in the cross-section increases as the slug structures are formed, with lower total oil content in the gas-core slug, as expected.

GCS have similar outer features to intermittent slugs but with a sustained central core structure. Fig. 1 shows images from the two types of slugs, namely full slug (a) and GCS (b). GCS are characterised by the liquid 'wrapping' up around the pipe from the stratified liquid followed by a sustained or intermittent gas core being present, while full intermittent slugs (FS) are formed by the rise of the interface while it remains roughly horizontal as if the pipe were being filled from below. FS may have gas-core entries or tails as described in [38].

Note that the cross-section images presented in Fig. 1 are reconstructed images from dielectric measurements, where the permittivity values are averaged for every pixel. Particles of size smaller than the pixels are not displayed.

The experimental measurements from ECT are analysed later in the manuscript by contrasting the spatial and temporal flow characteristics arising at various experimental conditions and comparing the reconstructed tomography images to published flow pattern classifications. Having characterised GCS, the next section describes the proposed methods exploiting ECT measurements to characterise such intermittent flow patterns.

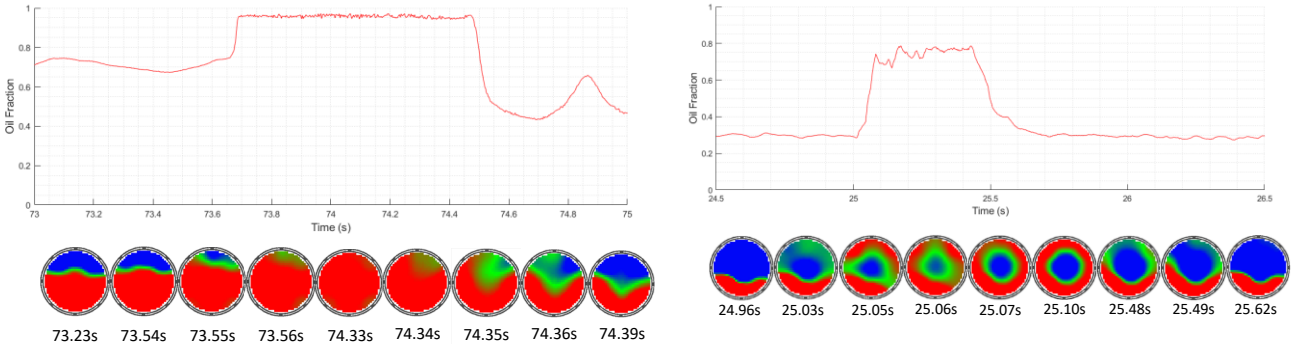

(a) (b)

Fig. 1. Illustration of the evolution of the volumetric fraction of (a) a full slug and (b) a gas-core slug at different times. The image correlates the cumulative oil volume fraction (top) to the instant phase spatial distribution along the cross-section (bottom) at given times. In the colour scheme, red symbolizes oil, blue is gas and green is the interface.

3. Method

The premise for flow pattern characterisation using ECT measurements is presented in this section. This work combines a high-level characterisation of the governing flow regimes in oil-gas mixtures, given particular test conditions, with a low-level automatic characterisation of intermittent structures. The detailed characterisation of slugs aims to provide a better understanding of the character of gas-core slugs and their transition from full-slugs. The overall methodology comprises the following stages:

a) Perform measurement using the ECT sensor array with various flowrates under controlled conditions,

b) Visually identify the governing flow regimes for every test point from ECT reconstructed images and transient mean oil fractions,

c) Juxtapose the identified flow regimes with existing flow pattern maps to quantify the prediction accuracy of the existing maps to the dataset,

d) Develop an algorithm for automatic differentiation of intermittent structures to characterise distinct spatial distributions,

e) Validate the algorithm.

3.1 Experimental setup

It has been discussed in Section 1 that the literature has focused on flow pattern maps derived from visual observations and that tomography imaging offers a non-intrusive alternative to flow pattern mapping. The use of tomography for assessment of various flow regimes aims to facilitate automation of online flow pattern recognition. To exploit the capabilities of ECT for flow pattern mapping, a series of experiments were conducted at the UK national standard multiphase flow loop at NEL in East Kilbride UK [37]. The test conditions and fluid properties are summarised in Table 2.

The experimental facility comprises a recirculation rig that uses gravimetric separation of the fluids (oil, gas and water) in continuous operation. The three-phase gravity separator located at the centre of the facility can separate 35 m^3 and 25 m^3 of water and oil respectively. The separator also acts as a storage vessel for the liquids undergoing testing.

Table 2. Experiment test conditions and fluid properties

Pressure (bar)	2-10
Temperature (°C)	20
Superficial velocity of oil (m/s)	0.10 – 4.8
Superficial velocity of gas (m/s)	0.25 – 8.9
Oil type	Paraflex HT9
Oil viscosity (cP)	15.9-17.9
Oil density (kg/m^3)	830 to 831
Gas type	Nitrogen
Gas density (kg/m^3)	3.4 – 13.8

A schematic of the loop showing the position of key components is illustrated in Fig. 2(a). The test section consists of a clear acrylic pipe with a total length of 8.5 m and 100 mm inner diameter. The liquid flows are recirculated around the test facility using variable-speed centrifugal pumps. The dry nitrogen gas is delivered at 12 bar at the injection point and then vented into the atmosphere from the separator after passing through the test section.

The flow rate of the gas in the test section is a function of the differential pressure between the testing section and the storage line. The reference measurements for both oil and gas flows are determined by the turbine flow meters after exit from the separation vessel. All experiments were conducted at controlled laboratory conditions at a temperature of 20 °C.

The ECT system installed on the test section, is shown in Fig. 2(b). The principle of operation of ECT is based on the sensitivity of the electrodes to changes in the dielectric properties of the fluids in the pipe. The different permittivity of the gas and oil leads to variations in the inter-electrode capacitance measurements. Each electrode-pair combination has an associated sensitivity matrix of 1024 pixels. The sensitivity matrix of each electrode-pair associates the change in the permittivity of a single pixel and the measured capacitance. Hence, the measurements from the sensors are directly proportional to the distribution of the dielectric properties within the pipe. For every frame, ECT measures 28 unique capacitance combinations from the pairs of electrodes placed around the perimeter of the pipe.

A commercial ECT unit was used, the system is detailed in [30]. The sensor array was arranged around the outside of the horizontal test section of the rig. The meter comprises 16 electrodes arranged in two measurement planes of 8 sensors each. The calibration of the ECT meter used single-phase flow of oil and gas in the pipe for reference measurements. The excitation signal was a 24 V peak to peak square wave at 2.5 MHz. The data were acquired at a frame rate of 354 Hz. Given the flow velocities, below 12 m/s, such a high-speed sampling rate, enables the characterisation of the multiphase structures without missing any relevant physical phenomena.

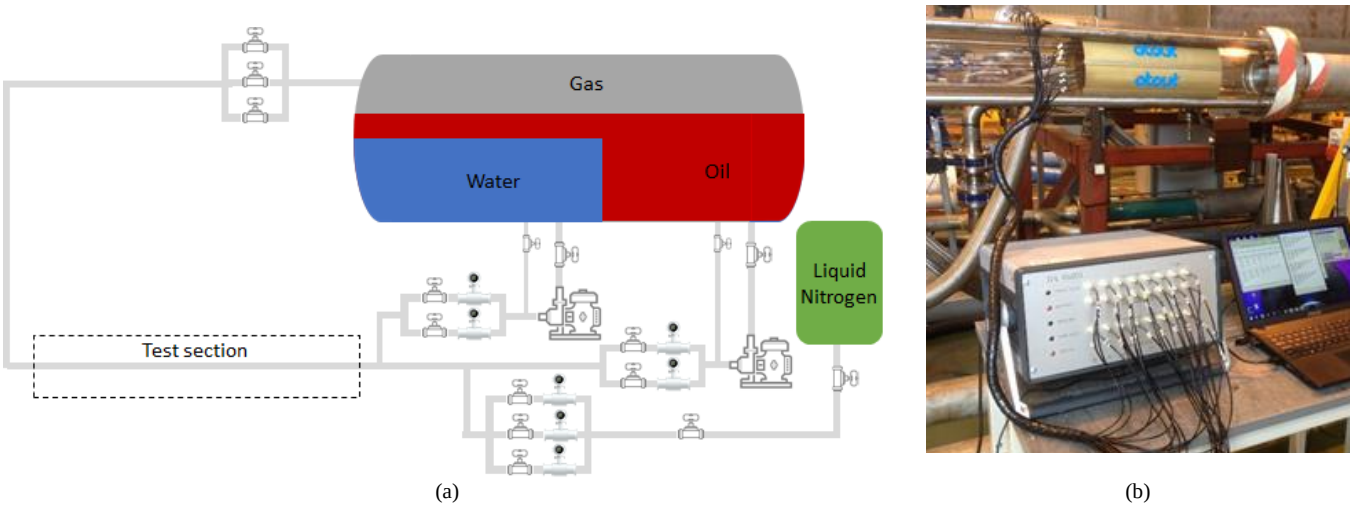

(a) (b)

Fig. 2. Illustration of the NEL multiphase flow facility Experiment showing (a) the schematic of the flow rig and (b) the measurement system working on the multiphase section

3.2 Identification of flow regimes from ECT

The flow regimes inside the pipe can be characterised according to specific flow-related parameters by combining the mean concentration in the measurement planes of ECT and the reconstructed cross-section images. The parameters available from electrical imaging, which are key indicators of horizontal flow structure, can be classified into spatial and temporal parameters. The spatial indicators are: average concentration of the liquid phase (holdup); spatial distribution of the concentration over the pipe cross-section; fluid level, range and balance of the probability density function of average concentration, e.g. (a) primarily liquid with gas bubbles present, (b) primarily gas with liquid structures passing or (c) fully intermittent slugs or waves. The temporal parameters comprise frequency distribution – number of structures passing in a given period; the primary structure velocity; and the length-scale of the primary structure. Based on these parameters and the unified flow pattern classification in Table 1, the data gathered during the experiments was characterised according to Table 3.

3.3 Prediction accuracy of flow regime maps

The accuracy of existing maps to predict the formation of the flow regimes identified through ECT was evaluated via the juxtaposition of the experimental data with the existing flow regime maps. The prediction accuracy of the eight flow pattern maps was assessed on our experimental data.

The dimensionless functions presented in Table 4 were used to compare the ECT-based characterisation to the regime zones in the maps. The dimensionless quantities used account for the Reynolds number, the Weber number and the Froude number. The Reynolds quantity correlates the effect of inertial to viscous forces, which is suitable to characterise transitions between segregated and distributed flows. The Weber number is useful for analysing the interface between two different phases, given by the correlation between the inertial forces to the surface tension. The Froude number derived from the ratio of inertial to gravity forces is strongly relevant for the analysis of wave structures.

Table 3. ECT parameters for flow characterisation

Parameter	(a) Segregated Stratified	(b) Segregated Wavy	(c) Intermittent Slug	(d) Intermittent Gas-core Slug.	(e) Intermittent Plug
Holdup	Low	Low	High	Medium-High	High
Spatial distribution	Segregated	Segregated	Segregated	Segregated	Segregated
Interface	Steady interface	Varying interface	Fully intermittent	Fully intermittent	Fully intermittent
Frequency	Low	Medium	High	Very high	Very high
Velocity	Low	Low	High	High	High
Length scale	N/A	High	Medium	Low	Low

Table 4. Dimensionless quantities for flow regime characterisation

Eaton et al. [5]	Two phase Reynold's function	$(N_{Re})_t = \frac{W_t {H_L}^2}{D\mu_t}$
	Two phase Weber function	$(N_{We})_t = \frac{\rho_L v_L {H_L}^{\frac{1}{2}}}{\gamma} + \frac{\rho_g v_s (1-H_L)^{\frac{1}{2}}}{\gamma}$
Beggs and Brill [4]	Froude Number	$Fr = \frac{u_m}{\sqrt{gD}}$
	Non-slip holdup	$\lambda = \frac{\mathrm{Q}_L}{Q_L + Q_g}$
Baker [6]	Baker's gas mass multiplier	$\tau = \sqrt{\frac{\rho_g}{\rho_a}\frac{\rho_w}{\rho_L}}$
	Baker's liquid-gas ratio multiplier	$\psi = \frac{\gamma_w}{\gamma_L}\left(\frac{\mu_L}{\mu_w} + \left(\frac{\rho_w}{\rho_L}\right)^2\right)^{\frac{1}{3}}$
Taitel-Dukler [3]	Lockhart and Martinelli parameter (Abscissa axis)	$X = \left[\frac{\frac{4C_L}{D}\left(\frac{U_{Ls}D}{\nu_L}\right)^{-n}\left(\frac{\rho_L (U_{Ls})^2}{2}\right)}{\frac{4C_G}{D}\left(\frac{U_{gs}D}{\nu_g}\right)^{-m}\left(\frac{\rho_g (U_{gs})^2}{2}\right)}\right]^{\frac{1}{2}}$
	Ordinate of frontier between (a)Stratified Wavy & annular (b) Stratified Wavy & Intermittent (c) Stratified Wavy & Stratified Smooth	$F = \sqrt{\frac{\rho_g}{\rho_L - \rho_g}}\frac{U_{gs}}{\sqrt{Gg\cos\alpha}}$
	Ordinate of frontier between Intermittent & Distributed Bubble	$T = \left[\frac{\frac{4C_L}{D}\left(\frac{U_{Ls}D}{\nu_L}\right)^{-n}\left(\frac{\rho_L (U_{Ls})^2}{2}\right)}{(\rho_L - \rho_g)g\cos\alpha}\right]^{\frac{1}{2}}$
	Ordinate of frontier between Segregated Stratified / Wavy	$K = \left[\frac{\rho_g U_{Ls} {U_{gs}}^2}{(\rho_L - \rho_g)g\ \nu_L \cos\alpha}\right]^{\frac{1}{2}}$

where W_t is the total mass ratio, H_L is the liquid holdup, D is the pipe diameter, μ_t is the total viscosity given by $\mu_t = {\mu_L}^{H_L}{\mu_g}^{(1-H_L)}$, ρ_L and ρ_g are the liquid and gas densities, respectively, v_L is the liquid velocity, $v_s$is the slip velocity given by $v_s = v_g - v_L$, U_{Ls} and U_{gs} are the superficial velocities of the liquid and gas phases, γ is the interface superficial tension, Q_L is the liquid flowrate, and Q_g is the gas flowrate. The subscripts a and w refer to the reference properties of air and water, respectively. Taitel-Dukler coefficient for turbulent flow are $C_L = C_G = 0.046$ and $n = m = 0.2$.

Using the dimensionless quantities above, the experimental data was arranged and plotted over the existing flow regime maps. The number of accurately predicted data points of every regime zone in each map was compared. This allows to assess the overall fitness of each mapping technique to our experimental data.

3.4 Flow regime characterisation algorithm

A logic-based algorithm for automatic slug structure differentiation was developed. The model extracts permittivity measurements from an ECT system. The algorithm compares the permittivity distribution along various cross-section areas of interest to identify the occurrence of intermittent structures for further flow pattern characterization.

For a given ECT permittivity measurement, at every time frame, an oil volume fraction is assigned to each pixel within the virtual 32x32 pixel-matrix across the cross-section. This volume fraction is calculated from the pixel permittivity using the extended Maxwell-Wagner-Sillars model as described in (1)

$$\varepsilon_m = \varepsilon_g \left[1 + n\alpha(\varepsilon_o - \varepsilon_g)/\left(\varepsilon_o + (n-1)\varepsilon_g - \alpha(\varepsilon_o - \varepsilon_g)\right)\right] \quad (1)$$

where ε_m is the mixture permittivity within each pixel, α is the fraction of oil in the same pixel, ε_o is the permittivity of the oil, ε_g is the permittivity of the gas. The mixture permittivity is itself derived from linear-back projection of the capacitance measured by the inter-electrode pairs calibrated against standard permittivities. n is a factor allowing for particle shape and which lies in the range 1 to ∞ [33].

The slug identification methodology relies on contrasting key parameters measured in different areas of the pipe cross-section to automatically identify and differentiate among various spatial phase distributions. The flow pattern recognition algorithm is based on grouping the cross-section pixels into 13 zones as illustrated in Fig. 3. This discretization follows the Nyquist–Shannon sampling theorem [39], which applied to image processing limits the dimensions of the zones to at least two times the size of the structures to be characterized.

The zonal discretization is suitable for velocity distribution calculation given that it is highly unlikely that the velocity of the fluid varies on a pixel-by-pixel basis in gas-liquid flow, yet it ensures that no actual information is lost in the analysis process. The velocity distribution tends to vary from structure to structure grouped by zones. The differentiation of gas-core slug from full slug flow was determined by contrasting the volume fractions, derived from the reconstructed permittivity distributions, measured at the centre of the pipe with those measured at various zones in the vicinity of the core, for each of the intermittent structures. This is based on the fact that gas-core slug flow accommodates a large void fraction in the centre of the pipe, zones 9 to 13, which corresponds to a lower permittivity measurement. Secluding the measurements from the zones of interest, pattern identification is feasible.

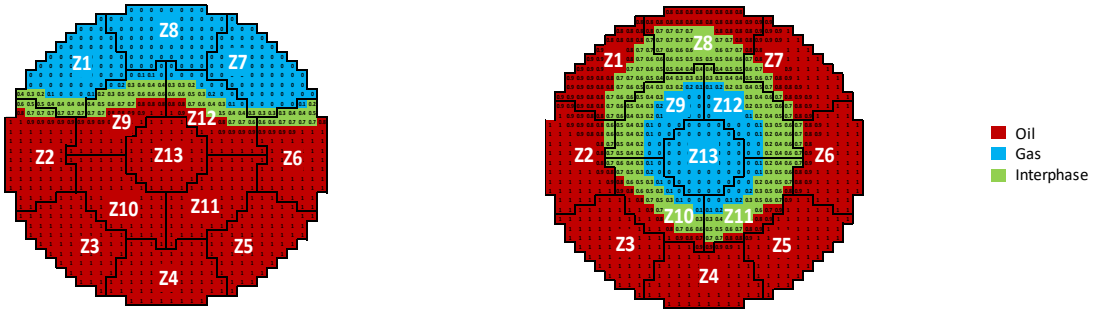

(a) (b)

Fig. 3. Zonal discretisation of the pipe cross section showing the oil volume fraction in every pixel for (a) a developing slug corresponding to t=73.23s in Fig. 3a, and (b) a gas-core slug corresponding to t=25.07s in Fig. 3b. Note that Z1 is zone 1, Z2 is zone 2, etc.

Fig. 4 shows the oil fraction measurements for two different datasets along 120 s of tests. The mean oil fraction across the pipe is plotted alongside the fractions in two other zones of interest, i.e. Zones 8 (top) and 13 (centre). Every peak in the trends corresponds to a structure passing though the measurement plane. Large differences are evident in the oil fraction between the two tests points, particularly for the central zone of the pipe.

Fig. 5 displays the instantaneous oil fraction of a randomly selected sample of 3540 frames corresponding to the datasets illustrated in Fig. 4. Fig. 5 illustrates the rule values used for characterising the flow regimes. The premise of the automated flow pattern differentiation between the full slug and gas-core slug flow are shown in Fig. 6 in accordance to the steps below.

i. Reconstruct a frame-by-frame image showing the relative permittivity distribution in every pixel via capacitance measurements over a given test period;

ii. Determine the frame-by-frame volumetric fraction image from the reconstructed permittivity distribution over a given test period. This is illustrated in Fig. 3, where for a given frame selected from the data in Fig. 1, the oil volumetric fraction in every pixel is populated across the entire cross-section;

iii. Deduce the occurrence of a gas-core slug or a full slug based on a set of rules relating to the fraction of oil and gas in selected zones of interest, e.g.:

a) A low volumetric fraction of oil (<0.2) in the pipe centre (this can be either zone 13, a subsection of zone 13, or zone 13 with subsections of adjacent zones, see Fig. 5f) combined with a high volumetric fraction of the oil (>0.8) in the near vicinity zones wrapping around the gas core (see Fig. 5e) indicates the occurrence of a gas-core slug. Note that a low threshold of oil volumetric fraction in the centre of the pipe ensures an appropriate characterisation of slugs with sustained gas core, by

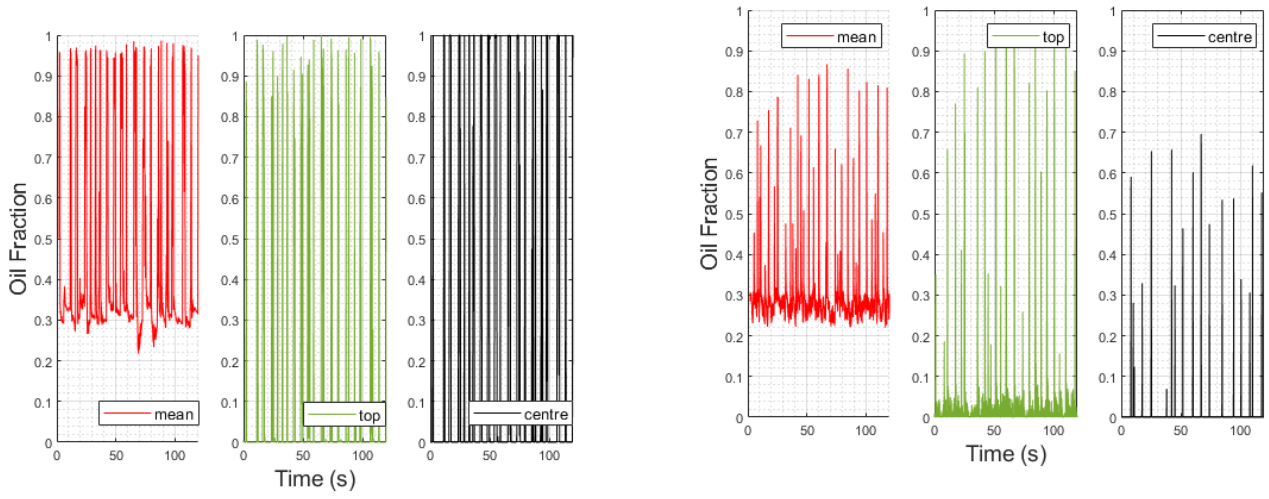

Fig. 4. Volume fraction measurements from cross-section (mean), the top of the pipe (Zone8) and the centre of the pipe (Zone13) for two different datasets (a and b)

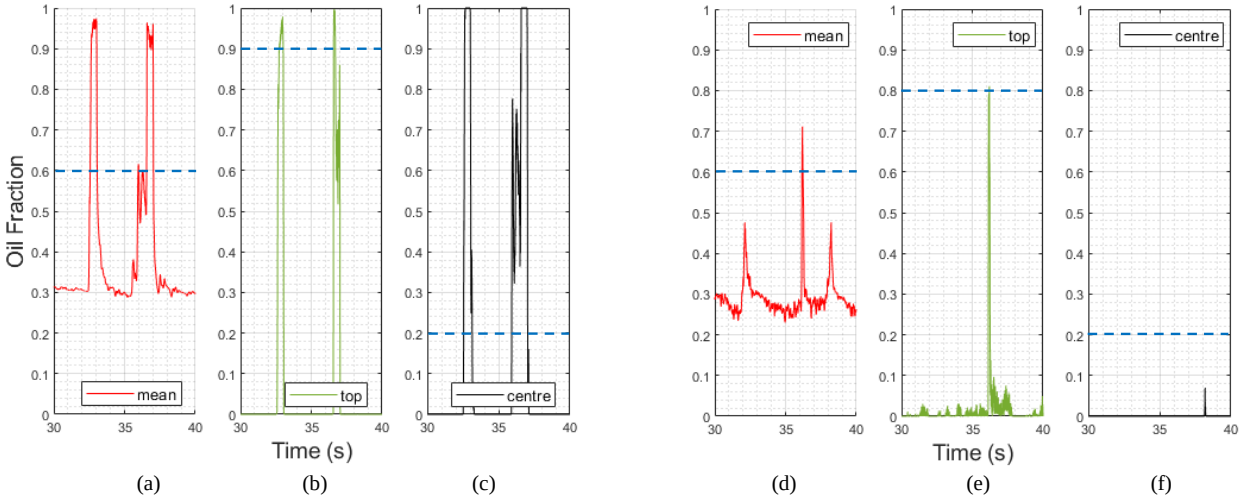

Fig. 5. Illustration of the premises used in the flow pattern detection algorithm showing the volume fraction measurements from a full slug (a, b and c) and a gas-core slugs (d, e, f) registered in the entire cross-section (mean), the top of the pipe (Zone8) and the centre of the pipe (Zone13).

disregarding aerated pseudo-slugs structures observed by other authors under high liquid and high gas superficial velocities conditions [8] [11] [14].

b) A consistent overall high value of the mean volumetric fraction of oil across all the imaging zones (>0.6) (see Fig. 5a) combined with a high volumetric fraction (>0.9) in at least a subsection of zone 8 (see Fig. 5b) over a number of the frames indicate an occurrence of the full slug.

iv. Compute the mean velocity for every structure considering the transit time of the front and tail between triggers. The slug length accounts for the time gap between triggers.

3.5 Measurement validation

The extended use of ECT for gas-liquid measurements has been addressed in Section 1. The accuracy of the ECT system used with regards to volume fraction computations was validated in previous work by contrasting the ECT measurements to reference weight measurements [16][40].

The flow regime characterisation algorithm was verified through blind tests. The validation tests consisted of comparing the algorithm outputs, i.e. number of structures, time of occurrence and length, to transient measurements to reconstructed images from three different test points. The algorithm rule selection is the most critical part of the algorithm. The rules represent the oil fraction values that split the data into three categories, the gas-core slug, the full slug, and non-slug. The rules were empirically tuned to ensure that no physical phenomenon was miscategorised during the structure discretisation.

Further validation of the algorithm output comprised comparison of the mean velocities and volume fractions of structures classified as gas core slugs with the Taitel-Barnea mechanistic transition criterion.

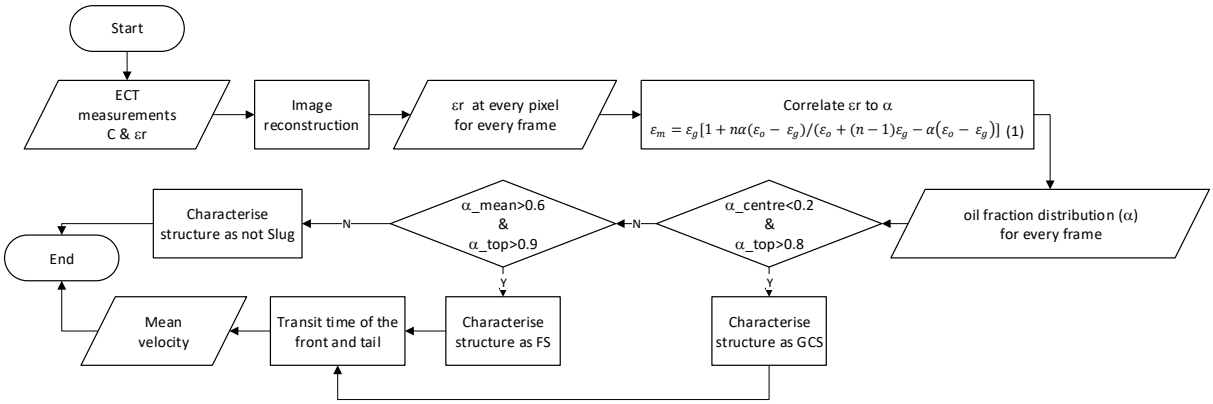

Fig. 6. Methodology for automatic flow regime characterisation showing the rules for the structures' characterisation. The variable C refers to the measured inter-electrode capacitance, ε_r is the relative permittivity, α is the oil fraction and the terms 'mean' 'centre' and 'top' refers to the zones in the pipe cross section, in accordance to Fig. 3, Fig. 4, and Fig. 5.

4 Results and discussion

4.1 Governing flow regimes from ECT measurements

The full range of the collected experimental data for the given phase superficial velocities is shown in Fig. 7. The data presented correspond to the governing flow characterisation performed from the ECT measurements in accordance with the classification parameters listed in Table 3. The classification of the data points in Fig. 7 shows the relationship between the identified flow patterns and the superficial velocities of both fluids. The majority of the flow regime transitions seen, i.e. between distributed, intermittent and segregated, are primarily influenced by the oil volumetric fraction. The transitions among the intermittent flows, including that to gas-core slug are predominantly driven by the velocity of the gas phase.

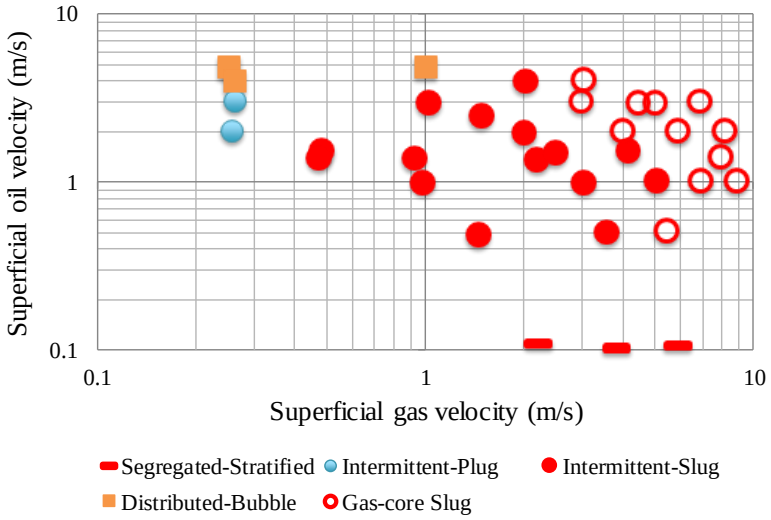

Fig. 7. Experimental dataset for the complete range of superficial velocities of the phases classified into flow regimes

4.2 Prediction accuracy of flow regime maps

Plotting the classified data from the experiments along the selected flow pattern maps yields the distributions in Fig. 8. The dimensionless maps derived by Beggs and Brill, Shell, and Eaton in Fig. 8(a), (b), and (c), respectively, account for a combination of dimensionless quantities and the Froude number. The association of the Froude number to wave structures makes it highly relevant for the study of regime transition between segregated and intermittent phases. The maps from Shell and Beggs and Brill, do not consider the effect of varying the fluid properties in the flow regime transitions. By contrast, the maps from Eaton and Baker, Fig. 8 (d), consider the density, viscosity and surface tension of the phases. Similarly to Fig. 7, the maps from NEL, Barnea, and Lin and Hanratty in Fig. 8 (f), (g), and (h), respectively, are based on the inflow quantities of the gas and liquid phases. The regime transitions in Taitel-Dukler map, in Fig. 8 (e), originates from theoretical methods avoiding the restrictions of empirical charts.

The overall data distribution presented in Fig. 8 (a), (c), (d) and (e) show that, as expected, the transition from stratified to intermittent has a downward trend with increasing liquid content. Fig. 8 (a), (c), (e) and (g) show a well-defined transition between distributed, intermittent, and segregated flows.

Quantification on the accuracy of the prediction of the experimental flow patterns is summarised in Table 5. The summary groups the intermittent-slug and the gas-core slug under a single cluster, labelled I-Slug. Results in Table 5 and Fig. 8 prove applicability of ECT to flow pattern characterisation. As shown in Fig. 8(e) the flow patterns identified with ECT characterisation fits well with the dimensionless map of Taitel-Dukler, which offers versatility with its semi-theoretical approach. A similar prediction accuracy was achieved by the Beggs and Brill dimensionless flow regime map (Fig. 8(a)), despite the evident differences between both experimental setups (refer to Table 2 and Appendix). This is because the combination of dimensionless parameters selected by Beggs and Brill to classify the flow pattern zones has enable it to provide acceptable results over a wider range of conditions. Conversely, the flow patterns seen using the ECT characterisation method seem to fall outside the flow regime maps of Baker and Lin and Hanratty, which are illustrated in Fig. 8 (c) and (h) respectively.

The Reynolds function used by Eaton [5] proved to be insignificant when the flow phases are in turbulent state yielding a negligible effect from the viscous forces. Likewise, the effect of variations in the fluid properties is non-relevant by contrasting the accuracy of Beggs and Brill and those from Eaton and Baker. This is attributed to the substantial difference between the properties of gas and liquid. This, however, may not be the case for mixtures with a less significant difference in the physical properties, i.e. liquid-liquid flows, where the effect of the properties of the fluids cannot be neglected.

Table 5. Predictive success of flow pattern maps

Map		S-Stratified	I-Slug	I-Plug	D-Bubble	Total
Taitel- Dukler	☑	2	27	2	3	34
	☒	1	0	0	0	1
Predictive success		*66.7%*	*100.0%*	*100.0%*	*100.0%*	*97.1%*
Beggs & Brill	☑	3	26	0	3	32
	☒	0	1	2	0	3
Predictive success		*100.0%*	*96.3%*	*0.0%*	*100.0%*	*91.4%*
Beggs & Brill-mod	☑	3	24	0	3	30
	☒	0	3	2	0	5
Predictive success		*100.0%*	*88.9%*	*0.0%*	*100.0%*	*85.7%*
NEL	☑	1	23	2	3	29
	☒	2	4	0	0	6
Predictive success		*33.3%*	*85.2%*	*100.0%*	*100.0%*	*82.9%*
Barnea	☑	3	19	0	3	25
	☒	0	8	2	0	10
Predictive success		*100.0%*	*70.4%*	*0.0%*	*100.0%*	*71.4%*
Shell	☑	0	18	0	0	18
	☒	3	9	2	3	17
Predictive success		*0.0%*	*66.7%*	*0.0%*	*0.0%*	*51.4%*
Eaton	☑	3	9	0	3	15
	☒	0	18	2	0	20
Predictive success		*100.0%*	*33.3%*	*0.0%*	*100.0%*	*42.9%*
Baker Mod	☑	0	0	0	3	3
	☒	3	27	2	0	32
Predictive success		*0.0%*	*0.0%*	*0.0%*	*100.0%*	*8.6%*
Lin & Hanratty	☑	0	0	0	0	0
	☒	3	27	2	3	35
Predictive success		*0.0%*	*0.0%*	*0.0%*	*0.0%*	*0.0%*

Regarding the gas-core slug flow, it is well defined by the Froude-holdup relationships as a subgroup within the intermittent region. This results in the Froude number and input liquid content being the most significant independent variables in gas-core slug flow characterisation. The relationship between these variables supports the characterisation of the gas-core slug flow in the following sections.

4.3 Intermittent regime sub-characterisation

The automatic algorithm is exploited in this section, with the aim of detailing the characteristics and evolution of the intermittent structures. Overall, 33 test points were evaluated, resulting in the identification of 4875 intermittent structures. Each measurement was made over a testing period of 120 s. The application of the algorithm detailed in Section 3.4 and illustrated in Fig. 6 classified 3393 structures as gas-core slugs (GCS) and 1482 structures as full slug (FS). A special phenomenon was observed during the data analysis, which is the occurrence of two types of gas-core slugs: fully developed gas-core slugs and developing slugs. At certain conditions, the gas-core slugs may evolve into regular full slugs or decay over time without further transition. For the purpose of this analysis, all structures are considered.

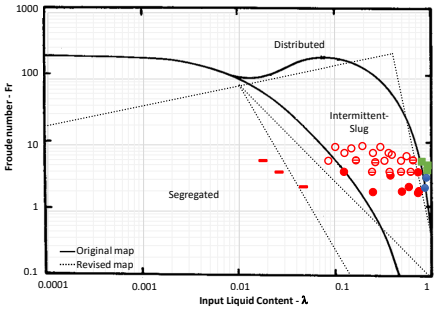

Beggs and Brill (1973) and Beggs and Brill revised

modified from [4], p612 and [35], p2

(a)

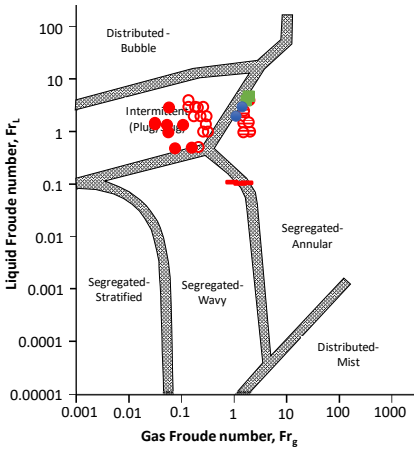

Shell (2007) modified from [20], p77

(b)

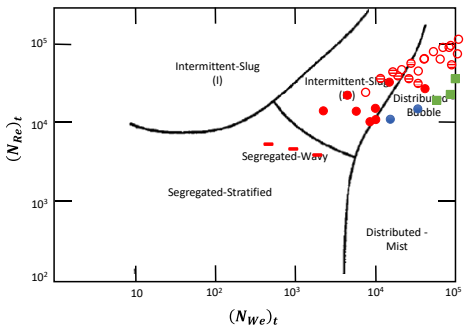

Eaton (1967) modified from[5], p823

(c)

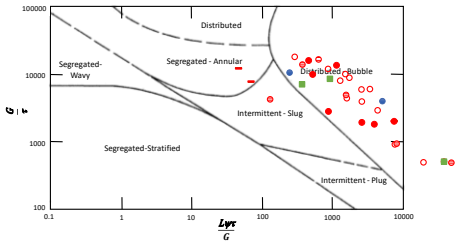

Baker (1953) modified from [6], p12

(d)

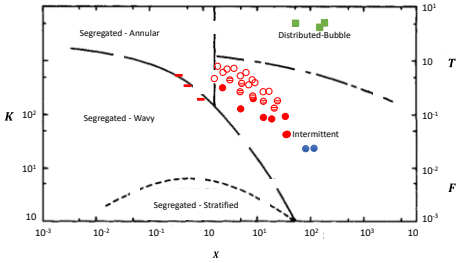

Taitel-Dukler (1976) modified from[3], p51

(e)

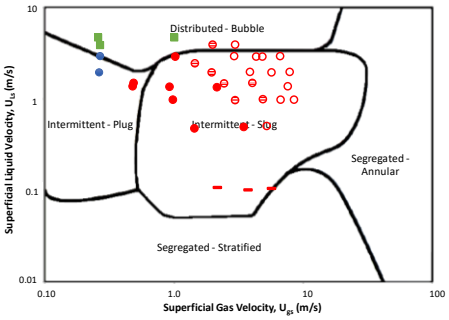

NEL map (1996) modified from [36][41], p62

(f)

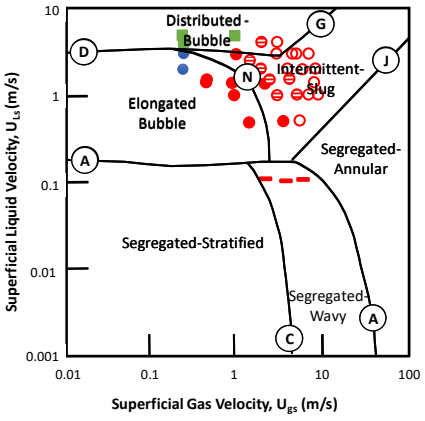

Barnea (1986) modified from [7], p4

(g)

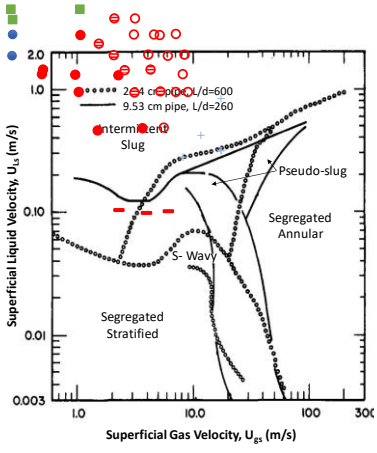

Lin and Hanratty (1987) modified from [8], p555

(h)

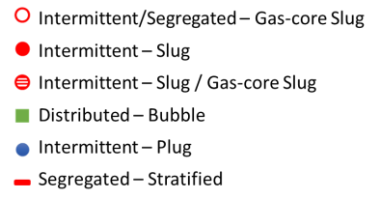

Fig. 8. Experimental data classification from ECT measurements adjoined with existing flow pattern maps showing the relationship between (a) non-slip holdup and Froude number, (b) gas and liquid Froude numbers, (c) Two-phase Weber function and Reynolds number, (d) Gas-mass and Gas-liquid ratios, (e) Lockhart and Martinelli and Taitel-Dukler transition parameters, and (f)-(h) gas and oil superficial velocities.

i. Number of structures

Fig. 9 (a) shows the number of GCS and FS, with the mixture velocity of all test points. The relationship between the number of intermittent structures and the velocity of the mixture is evident. At low mixture velocities, the intermittent structures are dominated by full liquid slugs. When the velocity increases above 6 $m.s^{-1}$, as a result of increasing gas velocity, only gas-core slugs take place within the pipe. Results suggest that for high mixture velocities gas-core slugs are not likely to transition to full slugs.

From Fig. 9 (b) it is noted that increasing the gas velocity decreases the number of FS structures. However, there is no evidence of the number of GCS being directly influenced by the superficial velocity of the gas phase.

In opposition to the effect of the gas superficial velocity on the occurrence of the intermittent structures, the upward trend in Fig. 9 (c) shows a clear relation to the increasing number of both FS and GCS. As the velocity of the oil increases, a larger number of structures are seen, with predominantly larger GCS structures for oil velocities beyond 2$m.s^{-1}$.

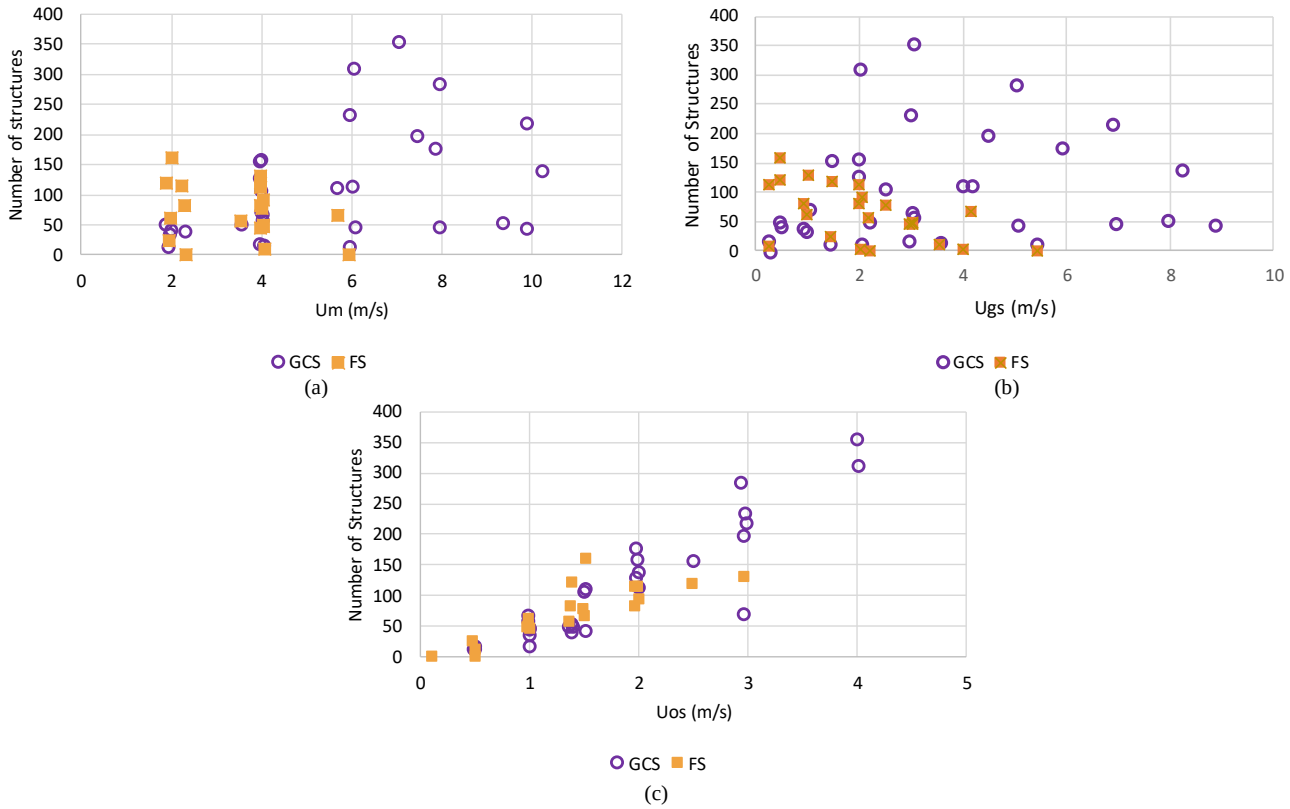

Fig. 9. Correlation between the number of intermittent structures and (a) the mean flow velocity; (b) the mean gas superficial velocity; and (c) the mean oil superficial velocity over a testing period of 120 s. Note that the superficial velocities are the total phase volume flowrate divided by pipe flow area.

ii. Structure span

The relationship between the span of the slug structures and the mean flow velocity is presented in Fig. 10. The time span of GCS structures was below 0.4 s throughout all testing conditions. The gas-core slug transition time was consistently under 0.2 s for the same condition at which full slugs transition time reaches up to 1 s.

Fig. 11 shows the evolution of the span of the GCS and FS structures with increasing superficial velocities. Results show that for a given mixture velocity, where both structures coexist, the length of the CGS increases with increasing gas velocity and that of the FS increases with increasing oil velocity.

iii. Slip velocity

Fig. 12 compares the oil fraction of a gas-core structure and the velocities of the phases in selected areas of interest. In fully developed gas-core slugs, the central region (Zone 13) contains mainly gas, whereas an oil layer exists around the perimeter of the pipe (Zones 1-8). The oil velocities at the bottom and top of the pipe, as well as the gas velocity in the central region are

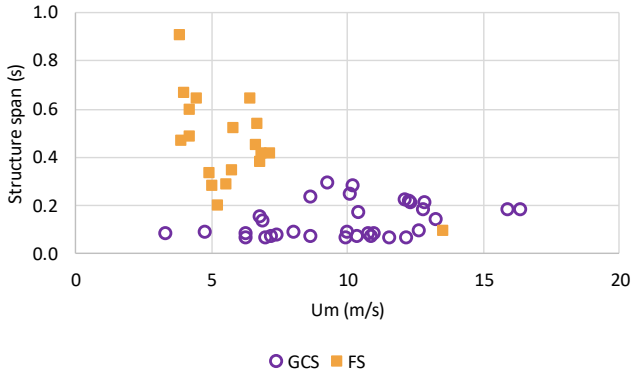

Fig. 10. Correlation between the mean duration of the structures and the flow velocity. Note that Um is the mixture superficial velocity or total volume flowrate divided by pipe flow area.

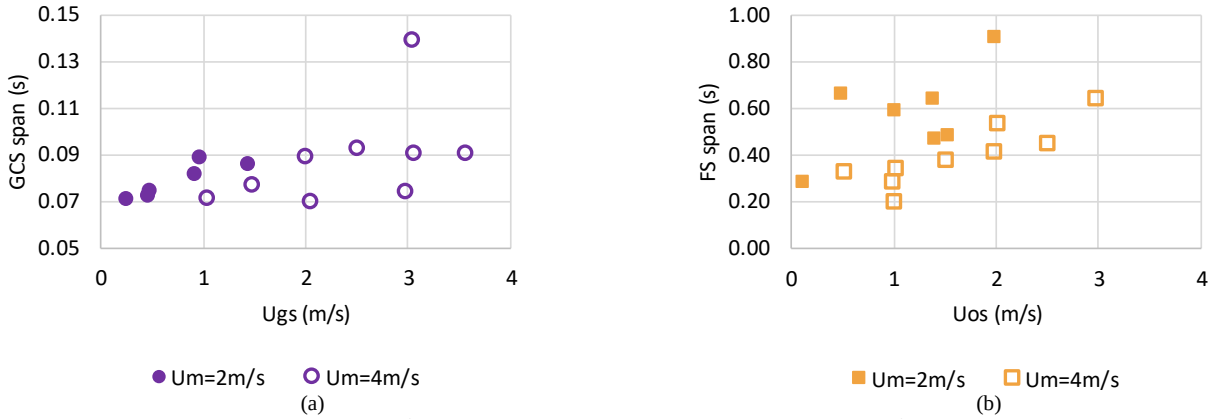

Fig. 11. Correlation between the structures length for various mixtures velocity correlating (a) the duration of the gas-core slugs (GCS span) and the gas superficial velocities and (b) the duration of the full-slugs (FS span) and the superficial velocity of the oil phase. Note that Um is the mixture superficial velocity or total volume flowrate divided by pipe flow area. Uos and Ugs are the oil and gas superficial velocities, respectively, given by the volume flowrate divided by the pipe flow area.

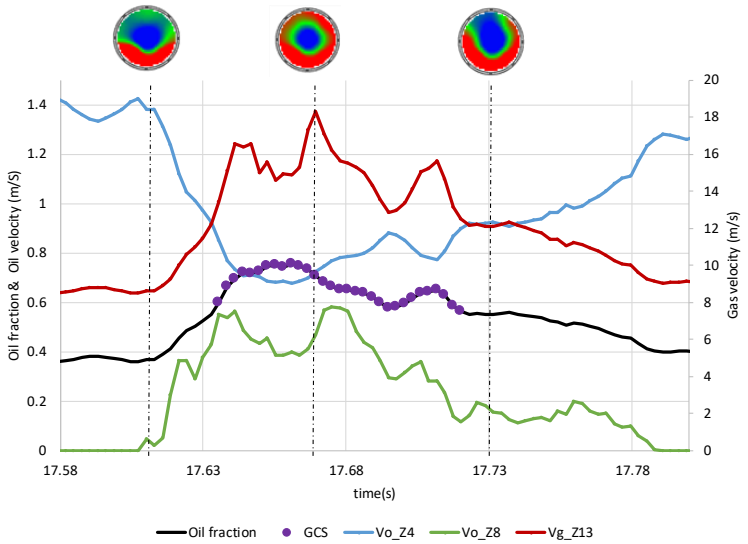

Fig. 12. Evolution of the oil fraction in a gas-core slug structure showing the velocities at the bottom (Zone4, V_{o_Z4}) and top of the pipe (Zone8, V_{o_Z8}), alongside with the gas velocity in the central region (Zone 13, V_{g_Z13}).

plotted in Fig. 12. The velocities shown are the effective phase velocity (V) in the zone given by:

$$V_{p\_Zi} = \frac{Q_{p\_Zi}}{A_{Zi}} \text{ for } i = \{1,2,\cdots,m\}\ (m = 13) \tag{2}$$

where the subscript p refers to the phase, i.e. gas or oil, and i is the index of the cross-section zone in accordance with the discretisation shown in Fig. 3. Q_{p_Zi} is the fraction of the phase 'p' in the Zone 'Z_i', and A_{Zi} is the area of the respective zone.

It is observed that as the liquid forms a film adhering to the perimeter and enveloping the central region, the velocity at the bottom (V_{o_Z4}) and the top (V_{o_Z8}) tend to have the same value while the GCS passes whereas the velocity of the central zone (V_{g_Z13}) rises as a result of the decreased area of gas flow. As the structure decays, and the gas-core breaks, the gas velocity decreases to its initial value.

Fig. 13 shows the evolution of a gas-core slug into a full slug structure. The zonal slip velocities between the gas and the oil phases are large for the gas-core slug but decrease substantially when the structure evolves to a full slug structure. This is seen in the zonal slip velocity between the oil and gas phases occupying the somewhat central zone 11.

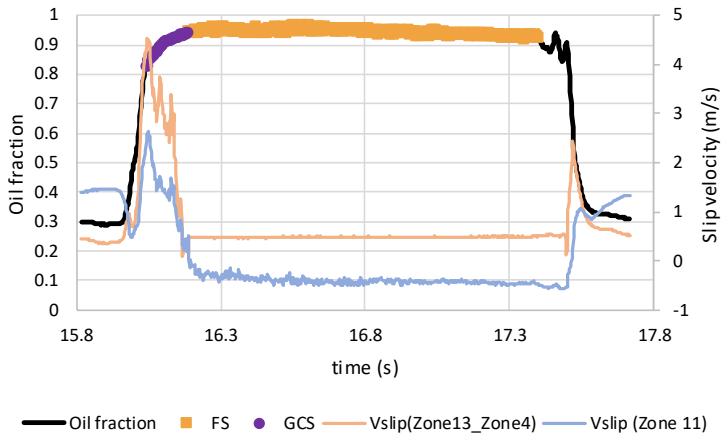

Fig. 13. Oil fraction of a gas-core slug evolving into a full slug structure showing the slip velocities between the gas at the core and the bottom of the pipe-Zone13 and Zone4, respectively- and of the gas and oil fractions occupying Zone 11.

The overall slip velocities of the oil and gas phases in full slugs and gas-core slugs of two data sets are compared as presented in Fig. 14. The flow in the data set 1 is dominated by full slugs. However, the occurrence of a number of gas-core slugs throughout the test allows comparison of the slip velocities for the same input conditions. It is observed that the slip velocities in gas-core slugs structures is much higher than the ones in full slug flow, as proposed in [15].

4.4 Gas-core slug prediction

i. Beggs and Brill-based transition model

Gas-core slug flow is well defined by the Froude-holdup relationships as a subgroup within the intermittent region, as shown in Fig. 8 (a). This confirms in the Froude number and input liquid content are key independent variables for characterisation of the gas-core slug structures. The relationship between these variables supports the characterisation of the gas-core slug flow based on the Beggs and Brill map.

The transition between the Intermittent-Slug flow and the Gas-core slug occurs for large liquid inflow and high inertial to gravity forces ratios, see Fig. 8 (a). From the Beggs and Brill map, the transition to gas-core slug flow is given by a straight line, the form of:

$$Fr = 4\lambda^{0.0021}, \qquad \lambda \in [0.0595, 0.6909] \tag{3}$$

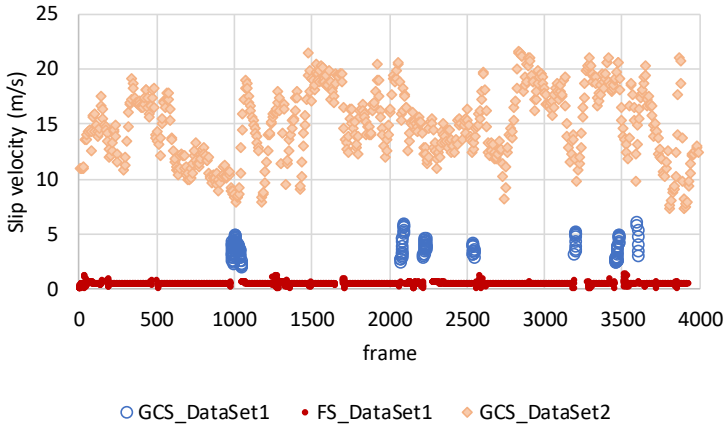

Fig. 14. Slip velocity in gas-core slug and full slug flow.

An extended analysis on the suitability of the transition model in (3) comprised the evaluation of all 4875 intermittent structures. The experimental data are plotted in Fig. 15, along with the transition criteria. It can be seen that for all test points but one, the transition criterion accurately differentiates GCS from FS.

ii. Taitel and Barnea combined prediction criterion

Departing from the empirical approach adopted by Beggs and Brill, Taitel and Dukler [3] suggested that the equilibrium liquid level in stratified flow is broken when the interphase surpasses the pipe centre. For a given liquid input, decreasing the liquid velocity results in an insufficient liquid flow to maintain the liquid slug, resulting in the liquid in the wave being swept up and around the pipe to form a gas core in the slug body.

Barnea [7] studied the transition mechanism from dispersed bubbles to intermittent slug flow as in (4). We now know from [8] and Fig. 8 (g) that the GCS occupies a region of transition between the distributed bubble and intermittent slugs. It is then logical to assume that when the bubble size is sufficiently large, they coalesce and form larger gas structures that, depending on the mixture velocity, could derive into GCS or FS.

$$d_c \geq \left[0.725 + 4.15\left(\frac{U_{gs}}{U_m}\right)^{\frac{1}{2}}\right]\left(\frac{\gamma}{\rho_L}\right)^{\frac{3}{5}}\left(\frac{2f_M}{D}{U_m}^3\right)^{\frac{-2}{5}} \tag{4}$$

where f_M refers to the friction factor, and d_c is the maximum diameter for stable disperse flow. The remaining terms are defined below Table 4.

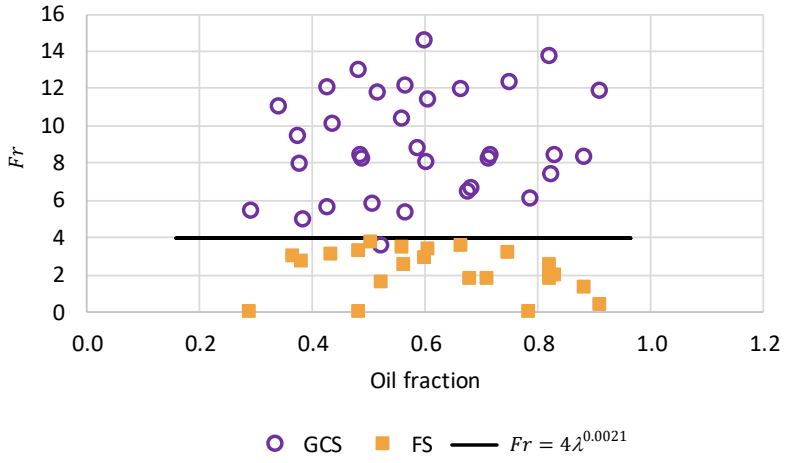

Fig. 15. Illustrating the suitability of the relationship between the Froude number (Fr) and the non-slip liquid holdup (λ), based on Begg and Brill modified map, to characterise the transition between full slug and gas-core slug-dominated flow.

The transition criterion in (4) was tested in the experimental data. Gas-core slug flow occurs when the critical bubble diameter, above which bubbles are deformed, is greater than the criteria defined by (4). Unifying the Taitel and Barnea transition mechanisms and applying it to our dataset results in an overall prediction of test condition where GCS structures govern the flow of 100%. Accordingly, gas-core slug flow arises when (5) is true.

$$2\left(\frac{0.4\gamma}{(\rho_L-\rho_g)g}\right)^{\frac{1}{2}} > \left[0.725+4.15\left(\frac{U_{gs}}{U_m}\right)^{\frac{1}{2}}\right]\left(\frac{\gamma}{\rho_L}\right)^{\frac{3}{5}}\left(\frac{2f_M}{D}{U_m}^3\right)^{\frac{-2}{5}} \quad (5)$$

The model in (5) was tested using the mean velocities and volume fractions measured for 2833 intermittent structures. The resulting classification was compared to that from the algorithm. Fig. 16 shows the agreement between the number of gas-core slugs and non-gas-core slugs, i.e. full-slugs in this case, classified using the algorithm described in Section 3.4 and the structure predictions using the model (5). Overall, the model coincided with the algorithm classification in 2630 structures, which corresponds to a 93% match. The quality of the prediction is greater than the predictive accuracy reported using the most recently developed semi-analytical algorithms (around 80%) and is within the same range as those using machine learning techniques (90-96%) [42].

Equations (3) and (5) define the occurrence of gas-core slug structures centred on dimensionless and dimension-based approaches, respectively. The prediction models allow the discretisation of the zones where, for a given flow condition, the gas-core-slug flow takes place.

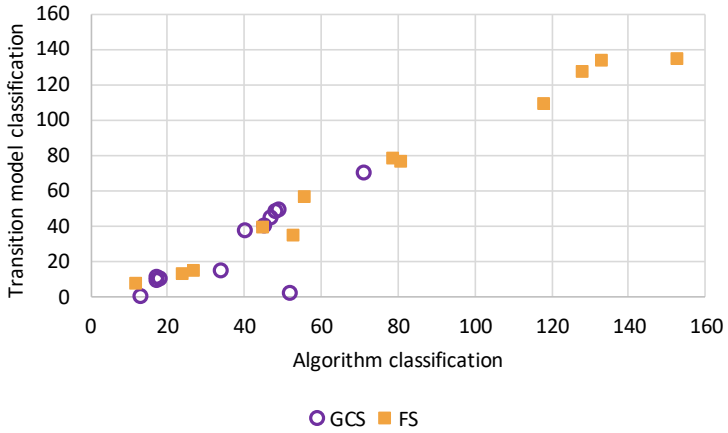

Fig. 16. Accuracy of the Taitel-Barnea transition criteria compared to reference slug classification from the automated algorithm

4.5 Revised flow pattern maps

This section proposes revisions to two flow pattern charts to accommodate gas core slug flow, as identified in this work, from the knowledge of flow variables. The boundaries on these charts represent transition zones between the observable flow patterns. The transitions respond to the equations (3) and (5). Since the existing flow regime maps do not account for gas-core slug structures in oil-gas flows, it is of interest to introduce this flow pattern explicitly.

In Fig. 17, the type of chart given by Beggs and Brill is reproduced, incorporating modifications to improve the agreement with the recent data and to include the novel gas-core slug flow. The intermittent flow area remains the same, but a sub-region is created where full slugs transition to gas core slugs. This transition is mainly dependent on the Froude number for a constrained range of liquid input rates.

Fig. 18 proposes a modification to the Taitel-Dukler map. The revision includes a gas-core slug zone as determined in (5). The dotted line of the form $F = -0.126\ \ln X + 0.5767,\ X \in [2, 90]$ gives the transition zone between gas slugs and gas-core slugs.

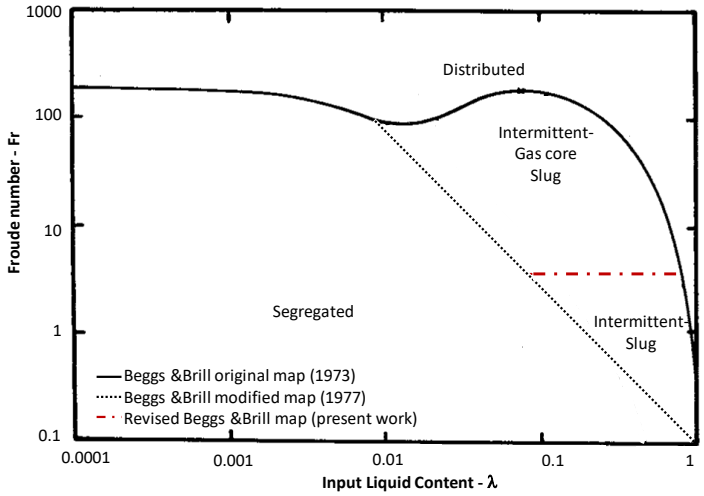

Fig. 17. Suggested flow pattern map for horizontal co-current flow showing the transition zones of Beggs and Brill original (1973), Beggs and Brill modified (1977) and the gas-core-slug transition proposed in the present manuscript

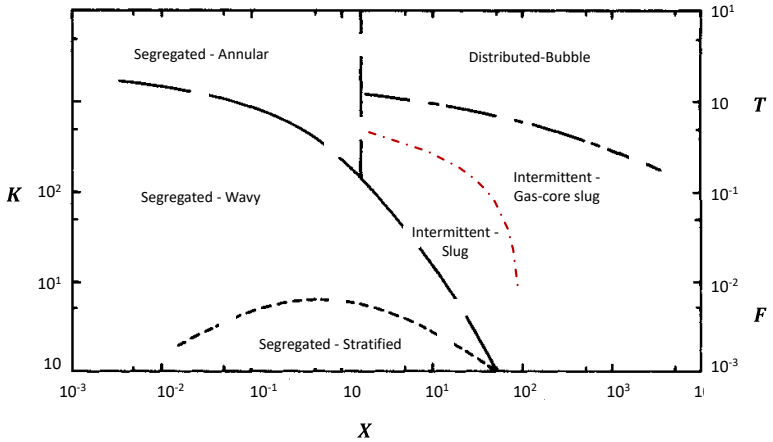

$$X = \left[\frac{\frac{4L}{D}\left(\frac{U_{Ls}D}{\nu_L}\right)^{-n}\left(\frac{\rho_L (U_{Ls})^2}{2}\right)}{\frac{4G}{D}\left(\frac{U_{gs}D}{\nu_g}\right)^{-m}\left(\frac{\rho_g (U_{gs})^2}{2}\right)}\right]^{\frac{1}{2}} \qquad K = \left[\frac{\rho_g U_{Ls} {U_{gs}}^2}{(\rho_L - \rho_g) g \nu_L \cos\alpha}\right]^{\frac{1}{2}}$$

$$T = \left[\frac{\frac{4L}{D}\left(\frac{U_{Ls}D}{\nu_L}\right)^{-n}\left(\frac{\rho_L (U_{Ls})^2}{2}\right)}{(\rho_L - \rho_g) g \cos\alpha}\right]^{\frac{1}{2}} \qquad F = \sqrt{\frac{\rho_g}{\rho_L - \rho_g}}\frac{U_{gs}}{\sqrt{Gg\cos\alpha}}$$

Fig. 18. Suggested flow pattern map modified from Taitel-Dukler for horizontal co-current flow, showing the transition between intermittent flows with a red dotted line

5 Conclusions

In this study, a unified flow regime discretisation is presented based on the published literature and recently studied intermittent flow structure, i.e., gas-core slug. The newly characterised intermittent flow structure has not previously been fully documented and differentiated in the vast majority of published flow regime maps, it is due to the difficulty in identifying the inner structure of slugs using the traditional optical methods.

The experimental results show that increasing velocity of the mixture for low liquid contents results in transitions from segregated to dispersed flows. Dispersion of gas bubbles in oil only occurs at low gas velocities and high liquid ratios. Intermittent flows are observed for liquid holdups above 10%. In these conditions, a transition between the slug and gas-core slug is observed as the Froude number increases. This phenomenon is attributed to increase of the gas phase velocity.

Reconstructed permittivity distribution of two-phase gas-liquid flow using high-speed electrical capacitance tomography enables identification of intermittent flow patterns in a pipeline without prior knowledge of the flow characteristics. An automated slug differentiation algorithm has been developed based on contrasting volumetric fractions in particular areas of the pipe cross-section.

A thorough evaluation of intermittent structures allowed characterisation of the gas-core slug flow. Full slug flow was found to decay above 6 $m.s^{-1}$, whereas gas-core slugs dominate intermittent flow for mixture velocities between 6 $m.s^{-1}$ and 10 $m.s^{-1}$. Gas-core slugs are, typically, shorter than full slug structures but are more frequent for the same given time period. In the case of gas-core slugs, the transition time is in an order of 0.05 second while for full slugs it is more likely to be 0.5 to 1 second.

The gas-core structures exhibit large gas-oil slip velocities when contrasted to full slugs. This is particularly evident in cases where gas-core slug flow evolves into full slug flow.

Transition models based on Beggs and Brill and Taitel-Barnea models were presented and validated with an accuracy of over 92%. Revisions to the Beggs and Brill and Taitel-Dukler flow regime maps are also proposed with consideration of gas-core slug flow. The presented revised flow-pattern maps are useful as it enables engineers to predict the nature of the flow pattern for a given case, and thus to design and to operate equipment accordingly.

The methodology proposed here for automatic slug differentiation has the potential to be extended for broader flow pattern classification, potentially with artificial intelligence or fuzzy logic.

The principle exploited, based on the spatial distribution of the fluid phases, makes the proposed method more robust and generalizable to other tomography methods. The automated flow pattern identification based on intrinsic fluid measurements has implications to enhanced flow measurement accuracy especially for those conventional flow meters which are flow regime dependent.

Acknowledgments

The data collection in this study was jointly funded by NEL, Coventry University and Atout Process Ltd. Special thanks to the team from NEL and Atout for undertaking the practical work and to iPhase Ltd for use of their analysis software.

References

[1] R. Thorn, G. a Johansen, and B. T. Hjertaker, “Three-phase flow measurement in the petroleum industry,” *Meas. Sci.*

Technol., vol. 24, pp. 1–17, 2012.

[2] G. Falcone, G. F. Hewitt, C. Alimonti, and B. Harrison, "Multiphase Flow Metering : Current Trends and Future Developments," *Soc. Pet. Eng.*, no. Distinguisehd author series, 2002.

[3] Y. Taitel and A. Dukler, "A model for predicting flow regime transitions in horizontal and near horizontal gas-liquid flow," *AIChE*, vol. 22, no. 1, pp. 47–55, 1976.

[4] D. Beggs and J. Brill, "A study of Two-Phase flow in inclined pipes," *J. Pet. Technol.*, 1973.

[5] B. Eaton, D. Andrews, C. Knowles, I. Silberberg, and K. Brown, "The Prediction of Flow Patterns, Liquid Holdup and Pressure Losses Occurring During Continuous Two-Phase Flow In Horizontal Pipelines," *J. Pet. Technol.*, 1967.

[6] O. Baker, "Design Of Pipelines For The Simultaneous Flow Of Oil And Gas," *Soc. Pet. Eng.*, 1953.

[7] D. Barnea, "A unified model for predicting flow -pattern transitions for the whole range of pipe inclinations," *Int. J. Multiph. Flow*, vol. 13, no. 1, pp. 1–12, 1987.

[8] P. Y. Lin and T. J. Hanratty, "Effect of pipe diameter on flow patterns for air-water flow in horizontal pipes," *Int. J. Multiph. Flow*, vol. 13, no. 4, pp. 549–563, 1987.

[9] L. Zhai, J. Yang, and Z. Meng, "Detection of transient gas-liquid flow structures in horizontal shale gas well using wire-mesh sensor," *J. Nat. Gas Sci. Eng.*, vol. 72, no. September, p. 103013, 2019.

[10] N. R. Kesana, M. Parsi, R. E. Vieira, B. Azzopardi, E. Schleicher, B. S. Mclaury, S. A. Shirazi, and U. Hampel, "Visualization of gas-liquid multiphase pseudo-slug fl ow using Wire-Mesh Sensor," *J. Nat. Gas Sci. Eng.*, vol. 46, pp. 477–490, 2017.

[11] A. Arabi, Y. Salhi, Y. Zenati, E. K. Si-ahmed, and J. Legrand, "On gas-liquid intermittent flow in a horizontal pipe : Influence of sub-regime on slug frequency," *Chem. Eng. Sci.*, vol. 211, p. 115251, 2020.

[12] A. Z. Hudaya, A. Widyatama, O. Dinaryanto, W. Endra, Indarto, and Deendarlianto, "The liquid wave characteristics during the transportation of air-water strati fi ed co-current two-phase fl ow in a horizontal pipe," *Exp. Therm. Fluid Sci.*, vol. 103, no. January, pp. 304–317, 2019.

[13] A. Soedarmo, Y. Fan, E. Pereyra, and C. Sarica, "A unit cell model for gas-liquid pseudo-slug flow in pipes," *J. Nat. Gas Sci. Eng.*, vol. 60, no. September, pp. 125–143, 2018.

[14] M. Parsi, B. J. Azzopardi, A. Al-sarkhi, N. R. Kesana, R. E. Vieira, C. F. Torres, B. S. Mclaury, and S. A. Shirazi, "Do huge waves exist in horizontal gas-liquid pipe flow ?," *Int. J. Multiph. Flow*, vol. 96, pp. 1–23, 2017.

[15] A. Hunt and D. Millington, "Multiphase Flow Measurement through Next-Generation tomographic visualisation technology," in *Upstream Production Measurement Forum*, 2016, no. UPM 16030.

[16] A. Hunt, J. Pendleton, and Y. Ladam, "Visualisation of Two-Phase Gas-Liquid pipe flows using electrical capacitance

tomography," in *7th Biennial ASME Conference on Engineering Systems Design and Analysis*, 2004.

[17] L. P. Golan and A. H. Stenning, "Two-phase vertical flow maps," *Proc Instn Mech Engnrs*, vol. 184, no. 3, pp. 108–114, 1969.

[18] J. M. Manhandle, G. A. Gregory, and K. Aziz, "A flow pattern map for gas-liquid flow in horizontal pipes," *Int. J. Multiph. Flow*, vol. 1, pp. 537–553, 1974.

[19] J. L. Trallero, C. Sarica, and J. P. Brill, "A Study of Oil / Water Flow Patterns in Horizontal Pipes," *SPE Prod. Facil.*, no. August, pp. 165–172, 1997.

[20] Shell Global Solutions International B.V., "Gas-Liquid separators- Type selection and design rules," no. December. Shell, pp. 1–100, 2007.

[21] D. Beggs and J. Brill, "A Study of Two-Phase flow in Inclined Pipes," *J. Pet. Technol.*, vol. 25, no. 05, 1973.

[22] L. S. Hansen, S. Pedersen, and P. Durdevic, "Multi-Phase Flow Metering in Offshore Oil and Gas Transportation Pipelines : Trends and Perspectives," *Sensors*, vol. 19, no. 2184, pp. 1–26, 2019.

[23] S. Zou, L. Guo, and C. Xie, "Fast recognition of global flow regime in pipeline-riser system by spatial correlation of differential pressures," *Int. J. Multiph. Flow*, vol. 88, pp. 222–237, 2017.

[24] J. Polansky and M. Wang, "Proper Orthogonal Decomposition as a technique for identifying two-phase flow pattern based on electrical impedance tomography," *Flow Meas. Instrum.*, vol. 53, pp. 126–132, 2017.

[25] L. P. M. Colombo, M. Guilizzoni, G. m Sotgia, S. Bortolotti, and L. Pavan, "Measurement of the oil holdup for a two-phase oil-water flow through a sudden contraction in a horizontal pipe," *J. Phys. Conf. Ser.*, vol. 501, 2013.

[26] A. Hunt, "Weighing without Touching : Applying Electrical Capacitance Tomography to Mass Flowrate Measurement in Multiphase Flows," *Meas. Control*, vol. 47, no. 1, pp. 19–25, 2014.

[27] B. J. Azzopardi, L. A. Abdulkareem, D. Zhao, S. Thiele, M. J. Silva, M. Beyer, and A. Hunt, "Comparison between Electrical Capacitance Tomography and Wire Mesh Sensor Output for Air / Silicone Oil Flow in a Vertical Pipe," *Ind. Eng. Chem. Res*, vol. 49, pp. 8805–8811, 2010.

[28] M. Zhang, Y. Li, and M. Soleimani, "Experimental Study of Complex-valued ECT," in *9th World Congress on Industrial Process Tomography*, 2018, pp. 19–24.

[29] X. Zhu, P. Dong, and Z. Zhu, "Gas-solids Flow Measurement in Cyclone Dipleg by Dual-plane Electrical Capacitance Tomography Sensor," in *9th World Congress on Industrial Process Tomography*, 2018, pp. 203–209.

[30] A. Hunt, "Industrial Applications of High-speed Electrical Capacitance Tomography," in *9th World Congress on Industrial Process Tomography*, 2018, pp. 857–864.

[31] R. Deloughry, M. Young, E. Pickup, and L. Barratt, "Cost Effective Loading of Road Tankers Using Process

Tomography," in *2nd World Congress on Industrial Process Tomography*, 2001, no. August, pp. 565–572.

[32] D. Pacho and G. Davies, "Application of Electrical Capacitance Measurements to Study the Collapse of Oil Foams," in *2nd World Congress on Industrial Process Tomography*, 2001, no. August, pp. 618–627.

[33] A. Hunt, L. A. Abdulkareem, and B. J. Azzopardi, "Measurement of Dynamic Properties of Vertical Gas-Liquid Flow," *7th Int. Conf. Multiph. Flow*, pp. 1–10, 2010.

[34] R. Yan and S. Mylvaganma, "Flow Regime Identification with Single Plane ECT Using Deep Learning," in *9th World Congress on Industrial Process Tomography*, 2018, pp. 289–297.

[35] R. Ibarra, I. Zadrazil, C. N. Markides, and O. K. Matar, "Towards a universal dimensionless map of flow regime transitions in horizontal liquid-liquid flows," in *11th International Conference on Heat Transfer, Fluid Mechanics and Thermodynamis*, 2015.

[36] M. Macdonald and T. Leonard, "Developing a Multiphase Reference Network to Support Well Optimisation & Flow Assurance," in *Offshore Technology Conference*, 2016.

[37] NEL, "Multiphase Flow Meassurment Test Facility." [Online]. Available: https://www.tuv-sud.co.uk/uk-en/about-tuev-sued/tuev-sued-in-the-uk/nel/our-services/activities/calibration-testing/multiphase-flow-meter-testing-and-calibration/advanced-multiphase-facility-amf. [Accessed: 04-May-2019].

[38] R. Drury, A. Hunt, and J. Brusey, "Identification of horizontal slug flow structures for application in selective cross-correlation metering," *Flow Meas. Instrum.*, vol. 66, no. June 2018, pp. 141–149, 2019.

[39] M. I. Robert J., *Introduction to Shannon Sampling and Interpolation Theory*. New York: Springer-Verlag, 1991.

[40] S. H. Stavland, Y. Arellano, A. Hunt, R. Maad, and B. T. Hjertaker, "Multimodal analysis of gas-oil intermittent structures in co-current horizontal flow," in *2020 IEEE International Instrumentation and Measurement Technology Conference (I2MTC)*, 2020.

[41] M. Macdonald and T. Leonard, "ENG58 Multiphase flow metrology in oil and gas production critical review of multiphase flow patter data," 2015.

[42] G. Mask, X. Wu, and K. Ling, "An improved model for gas-liquid flow pattern prediction based on machine learning," *J. Pet. Sci. Eng.*, vol. 183, 2019.

APPENDIX

Flow condition envelope of published flow pattern maps

Flow pattern map	Flow condition envelope
Beggs and Brill [4]	- Air – water flow - Q_g = [0 – 354] m^3/hr - Q_l = [0 – 6.8] m^3/hr - D = [25.4 – 38.1] mm - P = [2.4 – 6.6] barg
Shell [20]	- ρ_g = 8 kg/m^3 - ρ_l = 860 kg/m^3 - ν_g = 1.2·10−5 Pa s - ν_l = 1.6·10−4 Pa s - γ = 0.03 N/m - D = 500 mm - P < 90 barg
Eaton [5]	- Q_l = [7.9 – 874] m^3/d - Q_g/Q_l = [0 – 23510] m^3/ m^3 - SG_g = 0.611 - SG_l = [0.77; 0.865; 1.01] - μ_g = 0.012 cP - μ_l = [3.50; 13.50; 1.01] cP - γ = [0.026; 0.030; 0.066] N/m - D = [50.8; 101.6; 431.8] mm
Baker [6]	- Air – water flow - γ = 0.073 N/m - D = [0.254 – 1.016] mm - T = 20°C - P = [0 – 1] barg
Taitel-Dukler [3]	- Newtonian liquid–gas mixtures. - Negligible hydraulic gradient in the liquid at transition conditions. - Gazley criteria is used for smooth stratified flow - $C_L = C_G = 0.046$ and $n = m = 0.2$ (turbulent flow) - Transition between intermittent and Distributed-Annular occurs when the liquid holdup is 0.5.
Barnea [7]	- Air – water flow - D = [25.4; 51] mm - T = 25°C - P = 1 barg
Lin and Hanratty [8]	- Air – water flow - D = [25.4; 95.3] mm - P = 1 bara
NEL [36]	- ρ_g = 12.7 kg/m^3 - ρ_l = [830; 1050] kg/m^3 - μ_g = 0.0177 cP - μ_l = [16; 1.3] cP - D = 101 mm - T = 20°C - P = 10 bara